Observability-based Local Path Planning and Collision Avoidance for Micro Air Vehicles Using Bearing-only Measurements

Huili Yu, Rajnikant Sharma, Randal W. Beard, and Clark N. Taylor

Abstract— In this paper we detail an observability based path planning algorithm for Small and Miniature Air Vehicles (MAVs) navigating among multiple static obstacles. Bearing-only measurements are utilized to estimate the time-to-collision (TTC) and bearing to obstacles using the extended Kalman filter (EKF). For the error covariance matrix computed by the EKF to be bounded, the system should be observable. We perform a nonlinear observability analysis to obtain the necessary conditions for complete observability. We use these conditions to design a path planning algorithm which simultaneously minimizes the uncertainties in state estimation while avoiding collisions with obstacles. Simulation results show that the planning algorithm successfully solves the single and multiple obstacle avoidance problems for MAVs while improving the estimation accuracy.

I. INTRODUCTION

Small and Miniature Air Vehicles (MAVs) have the potential to perform tasks that are too difficult or dangerous for human pilots. For example, they can monitor critical infrastructure and real-time disasters, perform search and rescue, and measure weather in-storms [1]. For many of these applications, MAVs are required to navigate in urban or unknown terrain where obstacles of various types and sizes may hinder the success of the mission. MAVs must have the capability to autonomously plan paths that do not collide with buildings, trees or other obstacles. Therefore, the path planning and obstacle avoidance problems for MAVs have received significant attention [1]–[5].

The path planning problem can be grouped into global path planning and local path planning. Global path planning requires complete knowledge about the environment and a static terrain. In that setting a feasible path from the start to the destination configuration is generated before the vehicle starts its motion [6]. The global path planning problem has been addressed by many researchers with the three most common solutions being potential fields methods, roadmap methods and cell decomposition methods [7]. On the other hand, local path planning is executed in real-time during flight. The basic idea is to first sense the obstacles in the environment and then determine a collision-free path [1].

This paper cleared for public release, 88 ABW-11-0205

Huli Yu and Rajnikant Sharma are Graduate research assistant in Department of electrical and computer engineering, Brigham Young University, Provo, USA, (`huiliyu.yhl,raj.drdo`)`@gmail.com`

Randal W. Beard is Professor in Department of electrical and computer engineering, Brigham Young University, Provo, USA, `beard@byu.edu`

Sensors Directorate, Air Force Research Labs, USA, `clark.n.taylor@gmail.com`

Local path planning algorithms require sensors to detect obstacles. Among the suite of possible sensors, a video camera is cheap and lightweight and fits the physical requirements of small UAVs [1]. However, a single camera only provides bearings to obstacles, but it is necessary to estimate TTC to avoid collisions from obstacles. We use the extended Kalman Filter (EKF) to estimate the state of an obstacle, which includes TTC and bearing to obstacle, given the bearing measurement from the camera. The key idea presented in this paper is to maneuver the MAV to minimize the state estimation uncertainty while simultaneously avoiding obstacles. We will show that these two tasks are complementary, if the reachability conditions are satisfied. Planning trajectories that account for the information content in the environment is called as coastal navigation [8]. Our work is similar to coastal navigation, however, we focus on making a accurate local map of the environment in the body frame of the vehicle instead of vehicle localization. We use the local mapping technique in our previous work [9]–[11], which builds a polar map in the local-level frame of the MAV using the camera measurements directly without transforming to the inertial frame. However, instead of using both TTC and bearing measurements as in [9]–[11], in this work we only use bearing measurements to estimate both the TTC and bearing to obstacles. For this purpose we will use nonlinear observability theory developed by Hermann and Krener [12]. Observability is a measure of information available for state estimation. Song et al. [13] show that the EKF is a quasi-local asymptotic observer for discrete-time nonlinear systems, and that the convergence and boundedness of the filter are achieved when the system satisfies the nonlinear observability rank condition and the states stay within a convex compact domain. Observability analysis has been studied extensively for the purpose of estimation [14]–[16]. While Bryson and Sukkarieh [17] perform the observability analysis of SLAM and develop an active control algorithm, the observability analysis is not used to develop active control. The contribution of this paper is that we use the observability analysis to explicitly design the path planning algorithm. The main contributions of this paper are as follows.

- We build polar maps using the TTC, which are independent of the ground or air speed of the MAV.
- We perform the observability analysis of the state estimation process from bearing-only measurements and
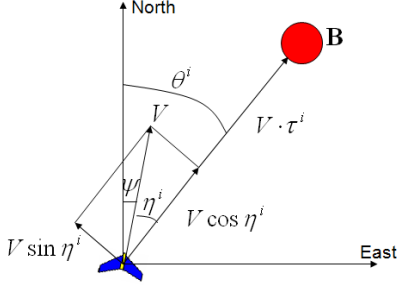
Fig. 1. This figure shows the motion of the ith obstacle relative to the MAV. The TTC and bearing to the obstacle are represented by τ^i and η^i. The ground speed is represented by V. The heading angle is represented by ψ. The angle between the line of sight of the obstacle and North direction is represented by θ^i. The location of the obstacle is represented by $\mathbf{B}$.
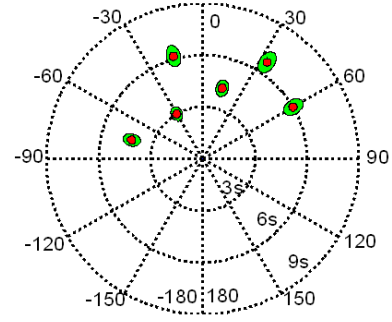

Fig. 2. This figure shows the local TTC map in the local-level frame of the MAV using polar coordinates. The origin of the map is the current location of the MAV. The circles represent the obstacles and the ellipses around them represent the TTC and bearing uncertainties. The radial direction is TTC in units of seconds.

find the necessary conditions for the observability of the system.

- We design a path planning algorithm based only on the local map around the MAV in the local-level frame.
- The algorithm minimizes the uncertainties in the TTC and bearing estimates while simultaneously avoiding obstacles.

The rest of the paper is organized as follows. Section II describes the model of the vehicle in the local-level frame and details nonlinear observability analysis. In Section III we describe the observability-based local path planning algorithm. Simulation results are provided in Section IV, and our conclusions are in Section V.

II. OBSERVABILITY ANALYSIS OF STATE ESTIMATION

In this section we will build a local map using the TTC to obstacles in the local-level frame of the MAV. The map is constructed in polar coordinates by estimating the TTC and bearing to obstacles. We perform a nonlinear observability analysis of the state estimation problem using bearing-only measurements, and find necessary conditions for complete observability of the system and establish a link between estimation accuracy and the minimum singular value of the observability matrix.

We assume the MAV is flying at a constant height above ground level. Since the obstacle map is in the local-level frame of the MAV, which is located at the origin, the equation of motion of each obstacle relative to the MAV needs to be derived. Let V represent the ground speed of the MAV and let ϕ and ψ represent the roll and heading angles, respectively. Figure 1 shows the motion of the ith obstacle relative to the MAV in the local-level frame, where τ^i and η^i are the TTC and bearing, θ^i is the angle between the line of sight of the obstacle and North direction, and $\mathbf{B}$ is the location of the ith obstacle in the local-level frame. Based on Fig. 1, the equations of motion of the obstacle relative to the MAV in terms of TTC and bearing are given by

$$\dot{\tau}^i = -\cos\eta^i, \tag{1}$$

$$\dot{\eta}^i = \frac{\sin\eta^i}{\tau^i} - \dot{\psi}, \tag{2}$$

where, assuming coordinated turn conditions, $\dot{\psi} = \frac{g}{V}\tan\phi$ and where ϕ is the roll angle of the MAV, which we assume to be a control signal. Since we use the camera to measure the bearing only, the measurement at time t is given by

$$z_t^i = \eta_t^i + v_t^i, \tag{3}$$

where v_t^i is the measurement noise that is assumed to be a zero-mean Gaussian random variable. Based on the state transition model expressed by Eqs. (1) and (2) and observation model expressed by Eq. (3), we use the EKF to estimate the TTC and bearing and build the local TTC map in the local-level frame using polar coordinates, as shown in Fig. 2. The origin of the map is the current location of the MAV. The circles represent the obstacles and the ellipses around them represent the TTC and bearing uncertainties.

In order to decrease the uncertainties in the TTC and bearing estimates, we analyze the observability of the system given by Eqs. (1), (2) and (3). Let $\mathbf{x}^i = [\tau^i, \eta^i]^\top$ represent the state vector associated with the ith obstacle. Let $\dot{\mathbf{x}}^i = \mathbf{f}(\mathbf{x}^i)$ and $z_t^i = h(\mathbf{x}_t^i)$ represent the state transition and observation models. The observability matrix is computed using Lie derivatives described by Hermann and Kerner [12]. The 0th order Lie derivative is $L_\mathbf{f}^0(h) = \eta^i$ and the 1st order Lie derivative is $L_\mathbf{f}^1(h) = \frac{\partial L_\mathbf{f}^0(h)}{\partial \mathbf{x}^i} = \dot{\psi} + \frac{\sin\eta^i}{\tau^i}$. We define the vector of Lie derivatives $\Omega = [L_\mathbf{f}^0(h), L_\mathbf{f}^1(h)]^\top$. The observability matrix is computed as

$$O^i = \frac{\partial\Omega}{\partial\mathbf{x}^i} = \begin{bmatrix} 0 & 1 \\ -\frac{\sin\eta^i}{(\tau^i)^2} & \frac{\cos\eta^i}{\tau^i} \end{bmatrix}. \tag{4}$$

The observability matrix has rank two if and only if $\tau^i \neq \infty$, $\eta^i \neq 2\pi p$ where $p \in \mathbb{Z}$. The EKF is a quasi-local asymptotic observer for nonlinear systems and its convergence and boundedness are achieved when the system is fully observable [13]. Bounds on the EKF error covariance P_t^i are related to the observability of the system given by Lemma 1 proved in [13].

Lemma 1 ([13]): Suppose that there exist positive real scalars α_1, α_2, β_1, β_2 such that $\beta_1 I \leq {O^i}^\top R^{-1} O^i \leq \beta_2 I$ and $\alpha_1 I \geq {C^i}^\top Q^{-1} C^i \geq \alpha_2 I$ then,

$$\left(\frac{1}{\beta_2 + \frac{1}{\alpha_2}} \right) \leq P_t^i \leq \left(\alpha_1 + \frac{1}{\beta_1} \right), \qquad (5)$$

where C^i is the controllability matrix, and Q and R are process and measurement noise covariance matrices.

From Lemma 1, we can see that both the maximum and minimum singular values β_1 and β_2 of the observability matrix should be maximized in order to minimize both the upper and lower bounds of the error covariance matrix. For the problem in this paper the order of system is two, and therefore minimizing the inverse of the determinant of ${O^i}^\top O^i$ will maximize the two eigenvalues of ${O^i}^\top O^i$. The determinant of the observability Grammian related to the ith obstacle is given by

$$\det({O^i}^\top O^i) = \frac{\sin^2 \eta^i}{(\tau^i)^4}. \qquad (6)$$

From Eq. (6), the inverse of determinant is given by $\frac{(\tau^i)^4}{\sin^2 \eta^i}$. It can be seen that for large τ, the inverse is high, which means observability is less, because change in the bearing measurement is very small with the TTC (low parallax). It can also be seen that the inverse is minimum at $\eta^i = \pi/2$ and is maximum when $\eta^i = 0$, meaning that the vehicle is moving directly towards the obstacle. Minimizing the inverse will ensure that $\eta^i \neq p\pi$ and will regulate $\eta^i \rightarrow \pi/2$. This implies that the minimization of the inverse of the determinant will minimize the lower and upper bounds of the error covariance matrix as well as steer the MAV away from the obstacle. Therefore the minimization of uncertainty and obstacle avoidance are complementary.

III. OBSERVABILITY-BASED PATH PLANNING

Based on the observability analysis in the previous section, we design the path planning algorithm such that (a) the MAV is maneuvered to the goal configuration and (b) the uncertainties in the TTC and bearing estimates are minimized, causing the MAV to avoid collisions. Let τ_t^g and η_t^g represent the TTC and bearing to the goal configuration at time t. Suppose that there exist n obstacles in the local map with bearing $|\eta_i| \leq \pi/2$, $i = 1, \cdots, n$. Let τ_t^i and η_t^i represent the estimated TTC and bearing of the ith obstacle. The determinant of the observability Grammian associated with the ith obstacle is given by $\det({O_t^i}^\top O_t^i) = \frac{\sin^2 \eta_t^i}{(\tau_t^i)^4}$. Let $\xi_t = [\tau_t^g, \eta_t^g, \tau_t^1, \eta_t^1, \cdots, \tau_t^n, \eta_t^n]^\top$. Define the utility $S : \mathbb{R}^{2n+2} \rightarrow \mathbb{R}$ as

$$S(\xi_t) = U_1 (\tau_t^g)^2 + U_2 (\eta_t^g)^2 + \sum_{i=1}^n W_i \frac{(\tau_t^i)^4}{\sin^2 \eta_t^i}, \qquad (7)$$

where U_1, U_2 and W_i, $i = 1, \cdots, n$ are positive weights. By minimizing the first two terms of S, the algorithm drives

the MAV towards the goal configuration. The third term of S penalizes the weighted sum of the inverse of the determinant of the observability matrices of all the n obstacles. By minimizing this term, the algorithm achieves two objectives simultaneously. First, it minimizes the uncertainties in the TTC and bearing estimates. Second, the MAV is steered around the obstacles. It is important to note that these two objectives are complementary to each other. We use the look-ahead policy over the horizon T to design the path planner. The cost function to be minimized is given by

$$J = \int_t^{t+T} S(\xi_\sigma) d\sigma. \qquad (8)$$

Before we show that the algorithm avoids obstacles successfully, we introduce the notion of reachability. Given the state $\mathbf{x}_t = [\tau_t^1, \eta_t^1, \tau_t^2, \eta_t^2, \cdots, \tau_t^n, \eta_t^n]^\top$ at time t, a pair $(\mathbf{x}_{t+T}, t + T)$ is said to be reachable from $(\mathbf{x}_t, t)$ over the horizon T, if it is possible to find a control function $\hat{\phi} : [t, t + T] \rightarrow U$, where U represents the set of control commands, such that along the resulting trajectory, $\eta_\sigma^i \neq 0$, $i = 1, \cdots, n$, $\forall \sigma \in [t, t+T]$. The reachable set $R_T(\mathbf{x}_t, t)$ from $(\mathbf{x}_t, t)$ over the horizon T, is defined as the set of points that are reachable from $(\mathbf{x}_t, t)$. The following theorem shows the MAV avoids collisions using this algorithm.

Theorem 1: If the reachable set $R_T(\mathbf{x}_t, t) \neq \emptyset$, for all $\mathbf{x}_t$ and t, then minimizing the cost function (8) ensures that the $\tau_t^i > 0$ for all obstacles and for all time. In other words, collision avoidance is guaranteed.

Proof: If the reachability condition is satisfied, then at each $(\mathbf{x}_t, t)$ at least one path over the look-ahead horizon T can be found such that along that path $\eta_\sigma^i \neq 0$, $i = 1, \cdots, n$, $\forall \sigma \in [t, t+T]$. This implies that at least one path can be found at each time such that the cost function J in Eq. (8) is finite along that path. Minimizing (8) ensures that η_σ^i remains bounded away from zero by a finite angle over the time horizon. Based on the collision triangle condition [18], collision will occur iff $\dot{\theta}_\sigma^i = 0$ and $\dot{\tau}_\sigma^i < 0$, where θ_σ^i is the angle between the line of sight to the ith obstacle in the inertial frame as shown in Fig. 1. Based on Fig. 1 and Eq. (2), we have that $\theta_\sigma^i = \eta_\sigma^i + \psi_\sigma$ and $\dot{\theta}_\sigma^i = \dot{\eta}_\sigma^i + \dot{\psi}_\sigma = \frac{\sin \eta_\sigma^i}{\tau_\sigma^i}$. Since minimizing (8) ensures that $|\dot{\theta}_\sigma^i|$ remains bounded away from zero, we are guaranteed that the minimum TTC over all obstacles remains bounded away from zero. ∎

We use dynamic programming to solve the optimization problem, however, other optimization tools could be used to solve the optimization problem. The focus of the paper is on the resultant path after optimization, and dynamic programming is just an optimization tool.

We discretize the time horizon T as the m-step look-ahead horizon $\{t, t + \Delta t, \cdots, t + m\Delta t\}$, where $\Delta t = T/m$. Let $k + i$, $i = 1, \cdots, m$ represent time instants $t + i\Delta t$. We also discretize U as a finite set of roll commands U_d. Eq. (8) then

becomes

$$J_d = \sum_{j=1}^{m} S(\xi_{k+j}). \tag{9}$$

We minimize J_d by recursively searching an m-step look-ahead planning horizon tree. The path planning algorithm can be described as follows. While the MAV executes the roll command at time step $k-1$ over the time interval Δt, the algorithm determines the optimal m-step look-ahead path $\gamma_k = \{\phi_k, \phi_{k+1}, \cdots, \phi_{k+m-1}\}$, where $\phi_{k+l} \in \mathcal{U}_d$, $l = 0, \cdots, m-1$, and the first roll command ϕ_k is applied. This process is repeated until the MAV reaches the goal configuration. Given an m-step look-ahead planning horizon tree, searching the tree and finding a path can be solved efficiently using dynamic programming [19]. The state transition models for the TTC and bearing expressed by Eq. (1) and (2) are the functions of the roll angle, which are denoted by $g_\tau(\phi)$ and $g_\eta(\phi)$. The TTC and bearing after the roll angle ϕ_k has been executed for a time interval Δt is given by

$$\tau_{k+1} = f_\tau(\tau_k, \phi_k) = \int_{k}^{k+\Delta t} g_\tau(\phi_k)dt + \tau_k, \tag{10}$$

$$\eta_{k+1} = f_\eta(\eta_k, \phi_k) = \int_{k}^{k+\Delta t} g_\eta(\phi_k)dt + \eta_k. \tag{11}$$

The state transition model for ξ_k is given by

$$\xi_{k+1} = \boldsymbol{\ell}(\xi_k, \phi_k) = \begin{bmatrix} f_\tau(\tau_k^g, \phi_k) \\ f_\eta(\eta_k^g, \phi_k) \\ f_\tau(\tau_k^1, \phi_k) \\ f_\eta(\eta_k^1, \phi_k) \\ \vdots \\ f_\tau(\tau_k^n, \phi_k) \\ f_\eta(\eta_k^n, \phi_k) \end{bmatrix}. \tag{12}$$

For each node at a certain step look-ahead horizon q, define

$$J^*(\xi_{k+q}, q) \triangleq \min_{\phi_j \in \mathcal{U}_d} \sum_{j=k+q}^{k+m-1} S(\boldsymbol{\ell}(\xi_j, \phi_j)). \tag{13}$$

Using the standard dynamic programming, J^* satisfies the recursion

$$J^*(\xi_{k+q}, q) = \\ \min_{\phi_{k+q} \in \mathcal{U}_d} (S(\boldsymbol{\ell}(\xi_{k+q}, \phi_{k+q})) + J^*(\boldsymbol{\ell}(\xi_{k+q}, \phi_{k+q}))) \tag{14}$$

with boundary constraint

$$J^*(\xi_{k+m-1}, k+m-1) = \\ \min_{\phi_{k+m-1} \in \mathcal{U}_d} S(\boldsymbol{\ell}(\xi_{k+m-1}, \phi_{k+m-1})). \tag{15}$$

Figure 3 shows an example of how the MAV path planning algorithm works using a two-step look-ahead planning tree, where each node has three children at the next step corresponding to three different roll commands. At time step k, the path $\gamma_k = \{\phi_k, \phi_{k+1}\}$ has already been found, as shown in Fig. 3(a). The roll command ϕ_k is applied. During the
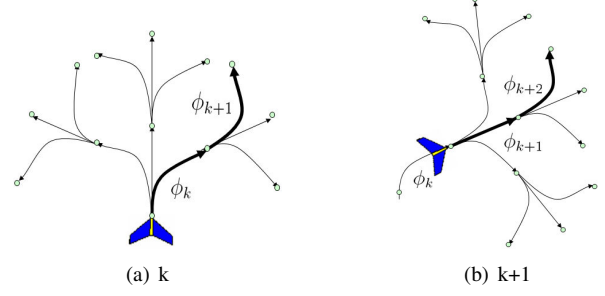

(a) k   (b) k+1

Fig. 3. This figure shows the two-step look-ahead path planning tree. Each node has three children. Subfigure (a) shows the optimal path $\{\phi_k, \phi_{k+1}\}$ is at time step k and subfigure (b) shows the optimal path $\{\phi_{k+1}, \phi_{k+2}\}$ at time step $k+1$.

period, the algorithm begins to build a new tree and to plan the new path $\gamma_{k+1} = \{\phi_{k+1}, \phi_{k+2}\}$ starting at time step $k+1$. Once the roll command has been executed, the new path γ_{k+1} has been generated, as shown in Fig. 3(b). The computation complexity of searching an optimal path using DP given the cost at each configuration is $O(\sum_{i=1}^{i=L} |U|^i)$, where $|U|$ is the size of the discrete control input and L is the number of horizon steps. This saves computation cost compared to exhaustive search, which gives $L|U|^L$.

IV. SIMULATION RESULTS

The algorithm was tested using a simulation environment developed in MATLAB/SIMULINK. The simulator uses a six degree of freedom model of the aircraft. The coordinate system is represented by NED (North-East-Down) system. The covariance matrices of the process and measurement noises are $Q = \begin{pmatrix} 0.001 & 0 \\ 0 & 0.0076 \end{pmatrix}$ and $R = 0.0012$. The weighting scalars U_1 and U_2 are 10 and 1. All the weighting scalars $W_i = 2$, $i = 1, \cdots, n$. Three-step look-ahead horizon path was planned with the sample interval $\Delta t = 1.2s$. We tested the algorithm for both single and multiple obstacle avoidance scenarios.

A. Single obstacle avoidance

In this scenario, the MAV was commanded to maneuver around an obstacle located at (150,250) between waypoint S (0,100,-40) and waypoint E (600,700,-40) represented by the box and plus signs shown in Fig. 4(a). Figure 4 shows the path followed by the MAV for avoiding the obstacle using the planning algorithm, the determinant of observability Grammian for that obstacle, the TTC and bearing, and the TTC and bearing error. It can be seen that when the determinant is maximum, then the bearing is $\eta = \pi/2$ and the TTC reaches its minimum value $\tau_{min} \approx 4s$. At the same time, the bound on the error covariance for the TTC is minimum, which shows that the uncertainties in state estimates can be minimized while simultaneously avoiding collisions.

B. Multiple obstacle avoidance

In the multiple obstacle avoidance scenario, the MAV was commanded to maneuver through twenty-five obstacles

(a) Inertial path

(b) Determinant

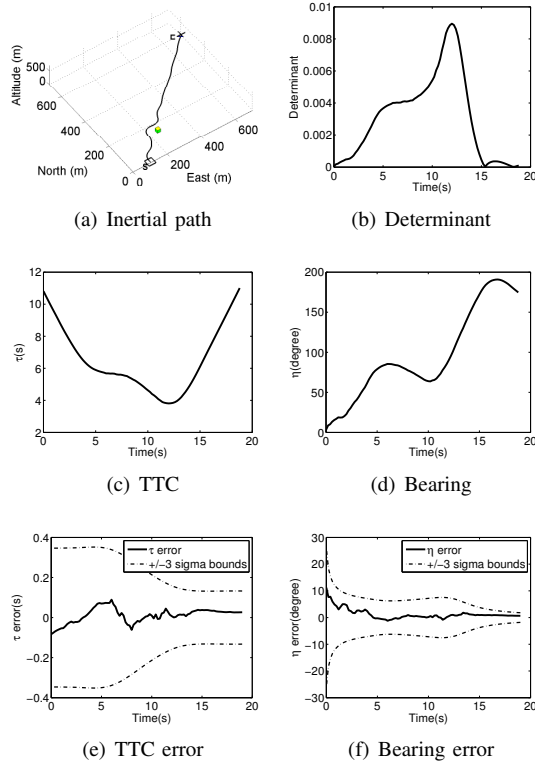(c) TTC

(d) Bearing

(e) TTC error

(f) Bearing error

Fig. 4. This figure shows the simulation results of single obstacle avoidance problem. Subfigure (a) shows the inertial path. Subfigure (b) shows the determinant of the observability Grammian. Subfigures (c) and (d) show the TTC and bearing to the obstacle. Subfigure (e) and (d) show the error and $\pm 3\sigma$ bounds of the error covariance for the TTC and bearing.

(a) t=20s
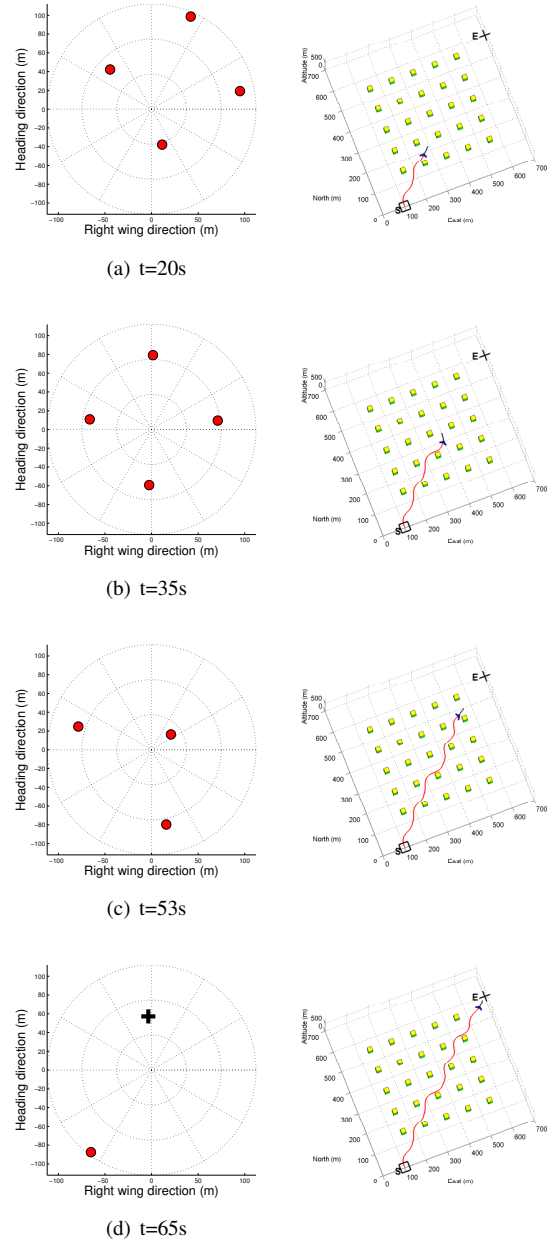
(b) t=35s

(c) t=53s

(d) t=65s

Fig. 5. This figure shows the evolution of the local map and the update of the path at different times. Subfigures on the left show the evolution of the local map. The dashed circles represent the TTC at 3s, 6s and 9s for inner, middle and outer circles respectively. Subfigures on the right show the path in the inertial frame. The black lines represent the three-step look-ahead paths and red lines represent the actual path followed by the MAV.

between waypoint S (0,100,-40) and waypoint E (600,700,-40), as shown in the subfigures on the right of Fig. 5. Figure 5 shows the evolution of the local map in the local-level frame and the update of the path in the inertial frame at different time steps. The dashed circles in the subfigures on the left represent the TTC at 3s, 6s and 9s for the inner, middle and outer circles respectively. The plus sign in subfigure (d) on the left represents the waypoint E in the local-level frame. Red lines in the subfigures on the right represents the paths followed by the MAV and black lines represent the optimal three-step look-ahead paths. Figure 6 shows the TTC and bearing to the obstacle located at (150,250), the TTC and bearing error, and the determinant of the observability Grammian of that obstacle. We can see that minimizing the cost function for multiple obstacle avoidance gives the same behavior for the obstacle avoidance, observability and further estimation uncertainties. Figure 7 shows how the value of the cost function changes as time progresses. Based on the figure, the cost function decreases initially when there are no obstacles in the local map. The cost function only consists of the first term. Once a new obstacle pops up, the cost function increases because the obstacle term is added to the cost function. The planning algorithm then minimizes the second term, causing the cost function to decrease. Once the collision is avoided and the obstacle is passed, it does not

add any cost to the cost function. The cost function then decreases based on the first term. Similar behavior occurs when multiple obstacles are observed.

V. CONCLUSIONS

This paper presents an observability based path planning algorithm for bearing only measurements. We perform the nonlinear observability analysis for state estimation and find that collision avoidance and uncertainty minimization prob-

(a) TTC   (b) Bearing

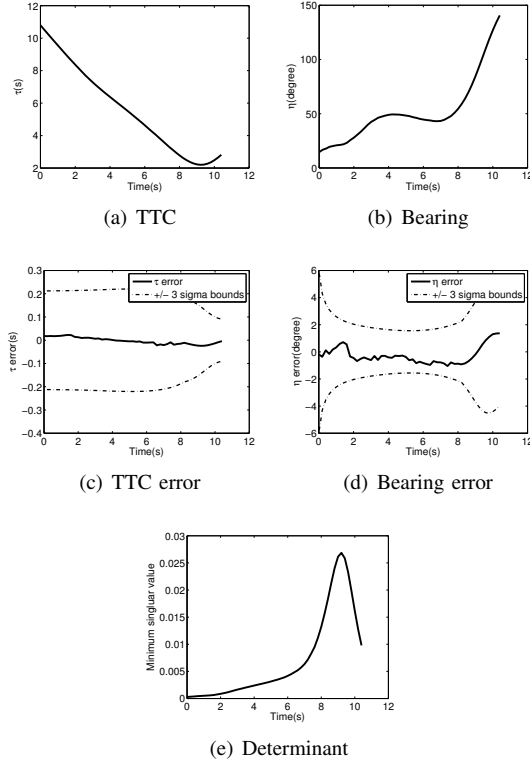(c) TTC error   (d) Bearing error

(e) Determinant

Fig. 6. This figure shows the TTC and bearing to the obstacle located at (150,250), the TTC and bearing tracking error and the determinant of the observability Grammian. Subfigures (a) and (b) show the TTC and bearing. Subfigure (c) and (d) show the error and $\pm 3\sigma$ bounds of the error covariance. Subfigure (e) shows the determinant of the observability Grammian.
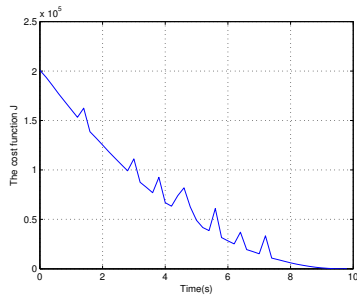

Fig. 7. This picture shows the value of the cost function as time progresses.

lem are complementary. Based on this analysis, we design the cost function that minimize the uncertainties of estimation while simultaneously avoiding obstacles. By minimizing the cost function, the path planning algorithm is developed directly in the local-level frame. We use the T time look-ahead policy to plan optimal paths. Simulation results show that the observability based path planner is successful in solving the single and multiple obstacle avoidance problems while improving the estimation accuracy.

In the paper, we use uniform weights for all the obstacles, which may not result in the best possible behavior. In the future, we will choose the weights based on the TTC and bearing to obstacles. We will also find the closed form solu-

tion for the minimum TTC between the MAV and obstacles using the algorithm. We will prove the global convergence of the planning algorithm which shows in which environments the algorithm can maneuver the MAV to the goal without causing any collisions.

VI. Acknowledgement

References

[1] B. Call, "Obstacle avoidance for unmanned air vehicle using computer vision," Master's thesis, Brigham Young University, December, 2006.

[2] A. Curtis, "Path planning for unmanned air and ground vehicles in urban environments," Master's thesis, Brigham Young University, 2008.

[3] E. Frazzoli, M. Dahleh, and E. Feron, "Real-time motion planning for agile autonomou vehicles," *Journal of Guidance, Control and Dynamics*, vol. 25, pp. 116–129, 2002.

[4] Y. Watanabe, E. Johnson, and A. Calise, "Vision-based approach to obstacle avoidance," in *Proceedings of the AIAA Guidance, Navigation, and Control Conference and Exhibit*, August 2005.

[5] A. Pongpunwattana and R. Rysdyk, "Real-time planning for multiple autonomous vehicles in dynamics uncertain environments," *AIAA Journal of Aerospace Computing, Information, and Communication*, vol. 1, pp. 580–604, December 2004.

[6] K. Sedighi, K. Ashenayi, R. Wainwright, and H. Tai, "Autonomous local path planning for a mobile robot using a genetic algorithm," *Congress on Evolutionary Computation*, vol. 2, pp. 1338–1345, June 2004.

[7] J. Latombe, *Robot Motion Planning*. Kluwer Academic Publishers, Boston, MA, 1991.

[8] N. Roy, W. Burgard, D. Fox, and S. Thrun, "Coastal navigation-mobile robot navigation with uncertainty in dynamic environments," in *Proc. IEEE Int Robotics and Automation Conf*, vol. 1, 1999, pp. 35–40.

[9] H. Yu, R. Beard, and J. Byrne, "Vision-based local multi-resolution mapping and path planning for miniature air vehicles," in *Proceedings of American Control Conference*, June 10-12 2009.

[10] ——, "Vision-based local multi-resolution path planning and obstacle avoidance for micro air vehicles," in *Proceedings of the AIAA Guidance, Navigation and Control Conference*, August 10 2009.

[11] ——, "Vision-based navigation frame mapping and planning for collision avoidance for miniature air vehicles," *Special Issue on Aerial Robotics, Control Engineering Practice*, vol. 18, no. 7, pp. 824–836, July 2010.

[12] R. Hermann and A. Krener, "Nonlinear controllability and observability," *IEEE Transactions on Automatic Control*, vol. 22, no. 5, pp. 728–740, Oct 1977.

[13] Y. Song and J. W. Grizzle, "The extended Kalman Filter as a local asymptotic observer for descrete -time nonlinear systems," *Journal of Mathemetical Systems, Estimation, and Control*, vol. 5, pp. 59–78, 1995.

[14] A. Martinelli and R. Siegwart, "Observability analysis for mobile robot localization," in *Proc. IEEE/RSJ International Conference on Intelligent Robots and Systems (IROS 2005)*, 2–6 Aug. 2005, pp. 1471–1476.

[15] I. Rhee, M. Abdel-Hafez, and J. Speyer, "Observability of an integrated GPS/INS during maneuvers," vol. 40, no. 2, pp. 526–535, April 2004.

[16] T. Vidal-Calleja, M. Bryson, S. Sukkarieh, A. Sanfeliu, and J. Andrade-Cetto, "On the observability of bearing-only SLAM," in *Proc. IEEE International Conference on Robotics and Automation*, 10–14 April 2007, pp. 4114–4119.

[17] M. Bryson and S. Sukkarieh, "Observability analysis and active control for airborne SLAM," *IEEE Transactions on Aerospace and Electronic Systems*, vol. 44, no. 1, pp. 261–280, January 2008.

[18] P. Zarchan, *Tactical and Stategic Missile Guidance*, 3rd ed. Washtington DC: AIAA Inc., 1997.

[19] F. Lewis, *Optimal Control*. New York: John Wiley and Sons, 1986.